Multidimensional Model for the Stress Analysis of Reinforced Shell Structures

A Multi-Dimensional Model for the Stress Analysis of Reinforced Shell Structures

Zappino Enrico[1] and Carrera Erasmo[2]
MUL^2 Team, Politecnico di Torino, Corso Duca degli Abruzzi, 24, 10129 Torino, Italy.

The present paper proposes an approach that can be used to mix one-, two- and three-dimensional refined models, derived using the Carrera Unified Formulation, to build a variable kinematic model that is able to deal with the static analysis of complex thin-walled structures. The adopted formulation, which only has displacements as degrees of freedom, allows these models to easily be connected to each other, that is, a variable kinematics model can be derived without *ad hoc* techniques. The refined models used in the present paper ensure high accuracy and low computational costs. The displacement continuity at the interface is guaranteed by the formulation, and no stress singularities appear in the kinematic model transition. The Mixed Interpolation Tensorial Component approach has been used, in a unified sense, for one-, two- and three-dimensional models to avoid the shear locking effect. The accuracy of the present approach has been confirmed by comparing the results with those from literature and with those obtained using commercial Finite Element codes. The static response of a reinforced panel and a section of an aircraft fuselage have been investigated to show the capabilities of the present approach. The use of refined structural models makes it possible to overcome the limits of classical structural models, and at the same time, to reduce the computational costs.

---

[1] Assistant Professor, Mechanical and Aerospace Engineering Department, Politecnico di Torino, Corso Duca degli Abruzzi, 24, 10129 Torino, Italy, enrico.zappino@polito.it.
[2] Professor, Mechanical and Aerospace Engineering Department, Corso Duca degli Abruzzi, 24, 10129 Torino, Italy, erasmo.carrera@polito.it. AIAA Senior Member.

I. Introduction

The development of efficient numerical models for structural analysis has the aim of providing accurate models with low computational costs. When thin-walled structures are considered, the structure can be seen as an assembly of different components: panels, ribs and longerons. Each of these components undergoes to different loads; panels are usually subject to shear stresses while longerons and ribs undergo to normal stresses. The *force method*, proposed by Argiris and Kelsey [2], exploited these assumptions to provide a solution to the elastic problem. The design approach introduced by Bruhn [7] was based on this method. The need to deal with complex geometries and the development of high-performance computers led to the introduction of the Finite Element Method, FEM [45]. Dozens of books are available on this method and the one by Zienkiewics deserves mentioning [49]. The FEM allows each structural component to be discretized into a finite number of elementary elements, and each of these can be analyzed using one- (beams/rods), two- (plates/shells) or three- (solids) dimensional elements. The kinematic assumptions of each element are derived from classical structural theories, such as those proposed by Euler [26] or Timoshenko [44] for the case of beams, or by Love [32], Reissner [38] and Mindlin [35] for the case of plates/shells. Three-dimensional models can be used to directly solve the equation of elasticity in their complete formulation, as shown by Argiris [1]. The accuracy of the results depends on the number of elements used to discretize the domain and on their kinematic assumptions, which means, an accuracy improvement requires an increase in computational cost. The use of solid models is obviously the best choice to obtain accurate results, but when thin-walled structures are considered, the use of three-dimensional elements requires a huge computational cost, that is, a different approach must be used. When reinforced thin-walled structures are considered, some approximate methods can be use. As an example, the reinforcements can be considered smeared over the plate; these approaches are presented in the works by Luan et al. [33] and Edalat et al. [24] but, in this case, the results do not provide detailed information about the behavior of each component of the structure. More detailed models have been presented by Mustafa and Ali [37] and Edward and Samer [25], who introduced some *ad hoc* finite element models that are able to deal with reinforced structures. The use of one-, two- and three- dimensional elements in the same model

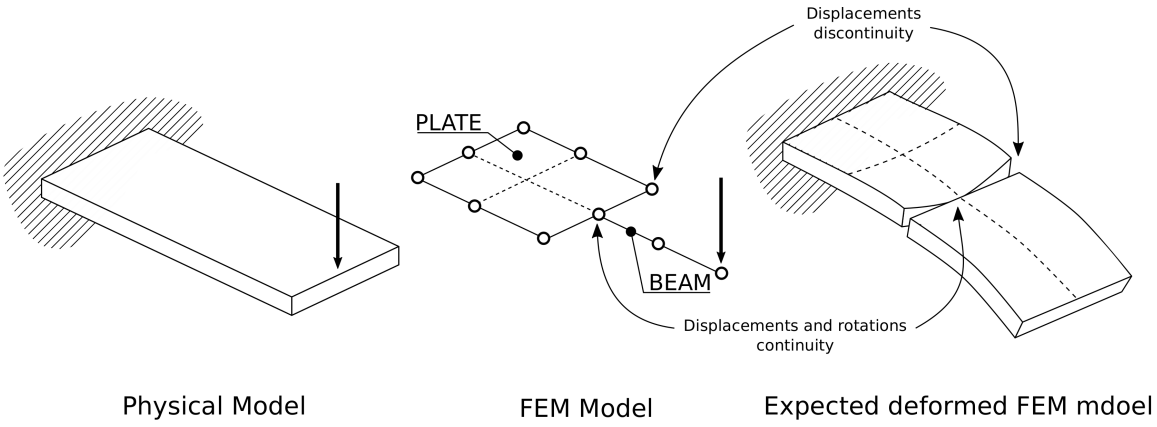

Fig. 1 Displacement discontinuities in a FEM model build using plate and beam elements.

can lead to a more efficient approach, which is able to provide accurate results with an acceptable number of degrees of freedom, DOFs. Classical FEM models approximate the kinematics using three displacements and three rotations at each node. This assumption is used for one- and two-dimensional elements, while three-dimensional elements only consider the three displacements. Even though, the unknowns of each finite element are expressed in a common manner, the coupling of these models could lead to discontinuities in the displacement field, as shown in Figure 1. Appropriate coupling techniques should be introduced to ensure an accurate solution. Surana [42, 43] proposed an approach to couple three and two-dimensional elements. The connection between solid and shell elements was also investigated by Liao et al. [31] and Cofer and Will [21]. The work by Gmür and Kauten [28] deals with the connection of solid isoparametric and super-parametric shell elements, while the connection between one- and three-dimensional elements was investigated by Gmür and Schorderet [29]. McCune et al. [34] and Monaghan et al. [36] introduced a mixed-dimensional coupling scheme, based on geometrical assumptions, while Garusi and Tralli [27] used a transition element to develop solid-to-beam and plate-to-beam connections. Song and Hodges [41] used an asymptotic approach to join beam and solid elements. A variational approach that is able to join incompatible kinematics was introduced by Blanco et al. [6]. Dávila [23] proposed a penalty method to join solid and shell elements, while Shim et al. [40] used multi-point constraint equations to force the congruence of the displacements at the interface of elements with different kinematics. Robinson et al. [39] proposed an automated approach for the development of mixed dimensional models starting from a Computer-Aided Design, CAD, model. Another technique used to derive

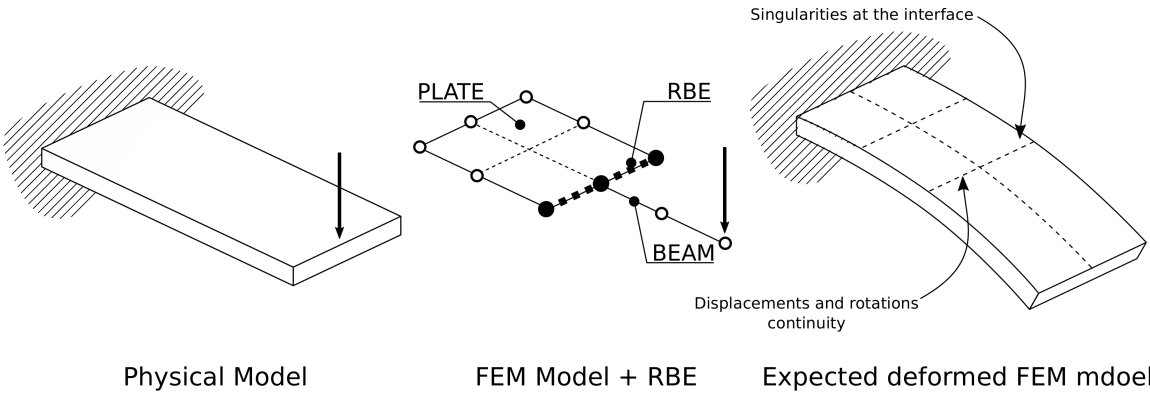

Fig. 2 Displacement discontinuities in a FEM model build using plate, beam and rigid body elements.

variable kinematic models is the *Arlequin* method which was first proposed by Ben Dhia [3], Ben Dhia and Rateau [4]. The *Arlequin* method couples two models and uses the overlapping zone where the transition is imposed. Classical FEM tools exploit special elements, the so-called Rigid Body Elements (RBE), see Figure 2, to connect a single node to multiple nodes in order to avoid discontinuities in the displacement field. This approach may lead to singularities in the stress field because, referring to the example in Figure 2, the plate has to follow the beam kinematics at the interface. This produces a constraint on the plate element that may create stress concentrations. The limitations introduced by classical structural models, such as the rigid section assumption in the case of beam models, can be overcome by refining the kinematic model, as shown in the review of advanced beam models presented by Carrera et al. [17]. When a refined formulation is used, the assumption of three displacements and three rotation in each node is not verified, in other words, the coupling between models with different kinematics becomes more complex. Hoseini and Hodges [30] proposed a technique to couple a beam mode, derived using a variable asymptotic approach [47, 48], and a solid element. The introduction of the Carrera Unified Formulation (CUF), which was proposed by the first author in Carrera [8, 9, 10] and which has recently been published in three books, see Carrera et al. [11, 13, 15], provides a unified approach that is able to derive variable kinematic models. CUF permits the equations of any refined 1D, 2D or 3D theory to be expressed in terms of a few fundamental nuclei, FNs, whose forms do not formally depend on the assumptions (type of functions or order) that have been used to describe the displacement field over the cross-section (in one-dimensional models) and through the thickness (in two-dimensional models). Biscani

et al. [5] proposed using the *Arlequin* method to couple variable kinematics elements derived using CUF. Carrera et al. [16] used the Lagrange multipliers to connect beam models derived with the same tool. A first attempt to connect structural elements with different kinematics, without *ad hoc* techniques, was firstly presented by Carrera and Zappino [19]. Subsequently the work proposed by Carrera and Zappino [20], a companion paper to the present manuscript, presented a general approach to build variable kinematic models, including one-, two- and three-dimensional elements, for the free-vibration analysis of complex structures. The present work exploits the models presented in the companion paper [20] and extends that approach to the static analysis of complex aeronautical structures.

Because the static analysis requires an accurate evaluation of the stress field, the shear locking correction has been improved using the Mixed Interpolation Tensorial Component approach, MITC. This approach was extended to CUF two-dimensional models by Carrera et al. [12] and to one-dimensional models by Carrera et al. [14]. The theoretical approach has been introduced in the first part of the present work, where a unified formulation for any kinematic model has been presented. A detailed comparison with classical FEM assembly approaches has been made to demonstrate the limits of these methods and how a higher accuracy solution can easily be obtained using refined models, such as the present ones. Several numerical results have been discussed and compared with those token from literature and those obtained using commercial FEM tools.

II. Variable kinematic finite elements

This section presents the method used to derive a unified and compact formulation for a class of finite elements with variable kinematics. The governing equations have been derived using the theory of elasticity while the Carrera Unified Formulation has been used to derive refined models in a compact and unified form. The numerical models have been exhaustively presented in detail in the book by Carrera et al. [13]. In this manuscript, the key-features have been reported to show how, the fundamental nucleus introduced by the Carrera Unified Formulation, is a direct consequence of the classical equilibrium equations.

A. Preliminaries

The fundamental equations and the nomenclature used in the following pages are introduced in this section. The displacement vector is denoted as follows:

$$\mathbf{u}^T = (u_{x_l},\, u_{y_l},\, u_{z_l}) \tag{1}$$

where u_x, u_y and u_z are the three components of the displacement vector expressed in the local reference system.

The strain and stress vectors are defined as:

$$\boldsymbol{\varepsilon}^T = (\varepsilon_{xx}, \varepsilon_{yy}, \varepsilon_{zz}, \varepsilon_{xy}, \varepsilon_{xz}, \varepsilon_{yz}), \tag{2}$$

$$\boldsymbol{\sigma}^T = (\sigma_{xx}, \sigma_{yy}, \sigma_{zz}, \sigma_{xy}, \sigma_{xz}, \sigma_{yz}). \tag{3}$$

The relation between the strains and displacements can be written using the geometrical equation:

$$\boldsymbol{\varepsilon} = \boldsymbol{b}\boldsymbol{u}, \tag{4}$$

where $\boldsymbol{b}$ is a differential operator, and its explicit form can be found in Carrera et al. [13]. Hooke's law permits the relation between stresses and strains to be derived:

$$\boldsymbol{\sigma} = \boldsymbol{C}\boldsymbol{\varepsilon}, \tag{5}$$

where $\boldsymbol{C}$ is the stiffness coefficients matrix of the material. When an isotropic material is considered,

matrix $\boldsymbol{C}$ can be written using Lamé's coefficients:

$$\boldsymbol{C} = \begin{bmatrix} \lambda+2G & \lambda & \lambda & 0 & 0 & 0 \\ \lambda & \lambda+2G & \lambda & 0 & 0 & 0 \\ \lambda & \lambda & \lambda+2G & 0 & 0 & 0 \\ 0 & 0 & 0 & G & 0 & 0 \\ 0 & 0 & 0 & 0 & G & 0 \\ 0 & 0 & 0 & 0 & 0 & G \end{bmatrix} \tag{6}$$

where

$$\lambda = \frac{E\nu}{(1+\nu)(1-2\nu)}, \quad G = \frac{E}{2(1+\nu)}. \tag{7}$$

where the symbol E denotes the Young's modulus while ν is Poisson's ratio.

B. Strong form of the equilibrium equation

The static equilibrium of a three-dimensional body subjected to a system of forces can be written for the three variations δu_x, δu_y and δu_z:

$$\begin{aligned} \delta u_x : &\frac{\partial \sigma_{xx}}{\partial x} + \frac{\partial \sigma_{xz}}{\partial z} + \frac{\partial \sigma_{xy}}{\partial y} = g_x \\ \delta u_y : &\frac{\partial \sigma_{yy}}{\partial y} + \frac{\partial \sigma_{yz}}{\partial z} + \frac{\partial \sigma_{yx}}{\partial x} = g_y \\ \delta u_z : &\frac{\partial \sigma_{zz}}{\partial z} + \frac{\partial \sigma_{zx}}{\partial x} + \frac{\partial \sigma_{zy}}{\partial y} = g_z \end{aligned} \tag{8}$$

where g_x, g_y, and g_z are the body forces. These equations, which are discussed in detail in any book regarding the Theory of elasticity, can be derived via kinematic assumptions, see da Silva [22], as well as by using the Principle of the Virtual Displacements, as shown by Washizu [46] and by Carrera et al. [13]. The solution of the elastic problem requires a stress field that is able to fulfill Equation 8 to be defined.

The equilibrium equation, here written in stress terms, can also be expressed in displacements

terms. Equation 8 can be written in compact form as:

$$\delta \boldsymbol{u}: \quad \boldsymbol{b}^T \boldsymbol{\sigma} = \boldsymbol{g} \tag{9}$$

Using Equation 5, the equilibrium equation assume the form:

$$\delta \boldsymbol{u}: \quad \boldsymbol{b}^T \boldsymbol{C} \boldsymbol{\varepsilon} = \boldsymbol{g}. \tag{10}$$

Finally, Equations 4 allows the equilibrium equation to be written in terms of displacements:

$$\delta \boldsymbol{u}: \quad \underbrace{\boldsymbol{b}^T \boldsymbol{C} \boldsymbol{b}}_{\boldsymbol{k}} \boldsymbol{u} = \boldsymbol{g}. \tag{11}$$

Matrix $\boldsymbol{k}$ is a 3×3 matrix, and it contains 9 differential operators,

$$\boldsymbol{k} = \begin{bmatrix} k_{xx} & k_{xy} & k_{xz} \\ k_{yx} & k_{yy} & k_{yz} \\ k_{zx} & k_{zy} & k_{zz} \end{bmatrix} \tag{12}$$

which, in explicit form, become:

$$\begin{aligned}
k_{xx} &= (\lambda + 2G)\ \partial_x \partial_x + G\ \partial_y \partial_y + G\ \partial_z \partial_z \\
k_{xy} &= (\lambda + G)\ \partial_x \partial_y \\
k_{xz} &= (\lambda + G)\ \partial_x \partial_z \\
k_{yx} &= (\lambda + G)\ \partial_y \partial_x \\
k_{yy} &= (\lambda + 2G)\ \partial_y \partial_y + G\ \partial_x \partial_x + G\ \partial_z \partial_z \\
k_{yz} &= (\lambda + G)\ \partial_y \partial_z \\
k_{zx} &= (\lambda + G)\ \partial_z \partial_x \\
k_{zy} &= (\lambda + G)\ \partial_z \partial_y \\
k_{zz} &= (\lambda + 2G)\ \partial_z \partial_z + G\ \partial_x \partial_x + G\ \partial_y \partial_y
\end{aligned} \tag{13}$$

The symbol ∂_x means a partial derivative with respect to x. The explicit form of the equilibrium equations, in terms of displacements, can be found in the book by Carrera et al. [13]. Although there are 9 terms in matrix $\boldsymbol{k}$, only 2 terms have a different structure. Let us consider the following two terms,

$$k_{xx} = +\left(\lambda + 2G\right)\ \partial_x\partial_x + \lambda\ \partial_z\partial_z + \lambda\ \partial_y\partial_y \tag{14}$$

$$k_{xy} = +\lambda\ \partial_x\partial_y + G\ \partial_y\partial_x \tag{15}$$

It is evident that the other components of matrix $\boldsymbol{k}$ can be obtained in a similar form as k_{xx} and k_{xy}. The elements on the diagonal have the form of k_{xx}, and the terms k_{yy} and k_{zz} therefore have the same form as k_{xx} but with the indices permuted. The elements outside the diagonal come from a permutation of the k_{xy} indices, and k_{xz}, k_{yz}, k_{yx}, k_{zx} and k_{zy} can in fact be obtained by permuting the indices in k_{xy}.

C. Weak form of the equilibrium equation

When the equilibrium equations are written in term of displacements, see Equation 11, the solution of the elastic problem requires a displacement field to be defined that is able to fulfill these equations at each point of volume V of the body. The closed form solution of these equations can only be obtained for simple geometries and boundary conditions. When complex problems have to be investigated, it is necessary to use the weak form. In a generic three-dimensional case the following can be written:

$$\boldsymbol{u}(x, y, z) = \Phi_i(x, y, z)\boldsymbol{u}_i, \tag{16}$$

where $\Phi_i(x, y, z)$ is a generic set of interpolating shape functions, while $\boldsymbol{u}_i$ are the unknown coefficients. When, as is usual, Lagrange functions are used $\boldsymbol{u}_i$ are the values of the displacements at the nodes.

The virtual variation of the displacements can be denoted as:

$$\delta \boldsymbol{u}(x, y, z) = \Phi_j(x, y, z)\delta \boldsymbol{u}_j. \tag{17}$$

The use of indexes i and j denotes summation. Using the principle of virtual work, it is possible to write:

$$\delta L_{int} = \delta L_{ext} \tag{18}$$

where L_{int} denotes the internal work while L_{ext} stands for the external work. δ is the virtual variation. The explicit form of the internal work is obtained using the equations introduced in the previous sections:

$$\delta L_{int} = \int_V \delta \boldsymbol{\varepsilon}^T \boldsymbol{\sigma} \, dV \tag{19}$$

If the generic displacement field reported in Equation 16 is considered and, the stress and strains are expressed according to Equations 4 and 5, the internal work becomes:

$$\delta L_{int} = \delta \boldsymbol{u}_j^T \underbrace{\left(\int_V \Phi_j \boldsymbol{b}^T \boldsymbol{C} \boldsymbol{b} \Phi_i dV \right)}_{\boldsymbol{k}^{ij}} \boldsymbol{u}_i = \delta \boldsymbol{u}_j^T \boldsymbol{k}^{ij} \boldsymbol{u}_i \tag{20}$$

$\boldsymbol{k}^{ij}$ is the fundamental nucleus of the stiffness matrix, it is a 3×3 matrix and it has a fixed form.

It is possible to compare the first two terms of the fundamental nucleus obtained in strong form, $\boldsymbol{k}$, reported in Equation 15, and the first two terms of the fundamental nucleus, $\boldsymbol{k}^{ij}$, derived in Equation 20. The first term assumes the form:

$$\begin{aligned} k_{xx} = \; & +(\lambda + 2G) \quad \partial_x \quad \partial_x \quad +G \quad \partial_y \quad \partial_y \quad +G \quad \partial_z \quad \partial_z \\ k_{xx}^{ij} = \; & +(\lambda + 2G) \int_V \Phi_{i,x} \Phi_{j,x} dV \; +G \int_V \Phi_{i,y} \Phi_{j,y} dV \; +G \int_V \Phi_{i,z} \Phi_{j,z} dV \end{aligned} \tag{21}$$

while the second can be written as:

$$\begin{aligned} k_{xy} &= +\lambda \quad \partial_x \quad \partial_y \quad + G \quad \partial_y \quad \partial_x \\ k_{xy}^{ij} &= +\lambda \int_V \Phi_{j,x}\Phi_{i,y}dV + G \int_V \Phi_{j,y}\Phi_{i,x}dV \end{aligned} \tag{22}$$

Equations 21 and 22 show how the fundamental nucleus, in weak form, is closely related to the strong form. Both the weak and strong forms are used to write an equilibrium equation, but only the former is satisfied at each point of volume V, while the latter is written in integral form and equilibrium is satisfied for mean quantities that originate from an integral of V.

D. Fundamental nucleus for 1D, 2D and 3D elements

The choice of the interpolating functions $\Phi_i(x, y, z)$ allows any kinematic assumption to be used to derive a structural model. One-, two- and three-dimensional elements are considered in classical Finite Element formulations. The next sections have the purpose of introducing these models in the form of the fundamental nucleus. The use of the fundamental nucleus will be used to easily introduce refined kinematic models that are able to overcome the limits of classical structural models.

1. Three-dimensional models

In the case of three dimensional models, the displacement field is approximated by only using the shape functions introduced by the FEM. As a result,

$$\boldsymbol{u}(x, y, z) = \Phi_i(x, y, z)\boldsymbol{u}_i = N_i(x, y, z)\boldsymbol{u}_i, \tag{23}$$

$$\delta\boldsymbol{u}(x, y, z) = \Phi_j(x, y, z)\delta\boldsymbol{u}_j = N_j(x, y, z)\delta\boldsymbol{u}_j, \tag{24}$$

where i ranges between 1 and the number of the expansion terms. If Lagrange functions are used, i ranges between 1 and the number of nodes of the element. In compact notation, the weak form of

the fundamental nucleus becomes

$$k_{xx}^{ij} = (\lambda + 2G) \int_V N_{i,x} N_{j,x} dV + G \int_V N_{i,z} N_{j,z} dV + G \int_V N_{i,y} N_{j,y} dV \tag{25}$$

$$k_{xy}^{ij} = \lambda \int_V N_{i,y} N_{j,x} dV + G \int_V N_{i,x} N_{j,y} dV \tag{26}$$

In the present paper, when the three-dimensional model has been considered in the analysis, 27 node iso-parametric solid elements have been used.

2. Two-dimensional models

The displacement field of a two-dimensional model can be written as the product of the finite element approximation on the reference surface, $N_i(x, y)$, and an expansion on the thickness direction, $F_\tau(z)$,

$$\boldsymbol{u}(x, y, z) = N_i(x, y) F_\tau(z) \boldsymbol{u}_{\tau i} \tag{27}$$

where $F_\tau(z)$ ranges between 1 and the number of terms of the expansion through the thickness. The fundamental nucleus can be written as:

$$\begin{aligned} k_{xx}^{\tau sij} =& (\lambda + 2G) \int_\Omega N_{i,x} N_{j,x} d\Omega \, dy \int_h F_\tau F_s dz + G \int_\Omega N_i N_j d\Omega \int_h F_{\tau,z} F_{s,z} dz + \\ &+ G \int_V N_{i,y} N_{j,y} d\Omega \, dy \int_h F_\tau F_s dz \end{aligned} \tag{28}$$

$$k_{xy}^{\tau sij} = \lambda \int_\Omega N_{i,y} N_{j,x} d\Omega \, dy \int_h F_\tau F_s dz + G \int_\Omega N_{i,x} N_{j,y} d\Omega \, dy \int_h F_\tau F_s dz \tag{29}$$

The integral over volume V can be written as the product of two contributions, that is, the integral over the reference surface, Ω, and the integral over the thickness, h.

In this work, a 9 node iso-parametric element has been used for the finite element formulation. One-dimensional quadratic Lagrange functions have been used as the thickness function, $F_\tau(z)$. More details about these models can be found in the book by Carrera et al. [13].

3. One-dimensional models

One dimensional models are characterized by an FE approximation on the axis, $N_i(y)$, and an expansion on the cross-section, $F_\tau(x,z)$,

$$\boldsymbol{u}(x,y,z) = N_i(y)F_\tau(x,z)\boldsymbol{u}_{\tau i}. \tag{30}$$

where $F_\tau(x,z)$ ranges between 1 and the number of terms of the expansion over the cross-section. Equations (14) and (15) can be written as

$$\begin{aligned} k_{xx}^{\tau sij} =&(\lambda+2G)\int_l N_iN_jdy\int_A F_{\tau,x}F_{s,x}dA + G\int_l N_iN_jdy\int_A F_{\tau,z}F_{s,z}dA + \\ &+ G\int_l N_{i,y}N_{j,y}dy\int_A F_\tau F_s dA; \end{aligned} \tag{31}$$

$$k_{xy}^{\tau sij} =\lambda\int_l N_{i,y}N_jdy\int_A F_\tau F_{s,x}dA + G\int_l N_iN_{j,y}dy\int_A F_{\tau,x}F_s dA \tag{32}$$

The integral over volume V can be split into the integral over the cross-section, A, and the integral along the beam axis, y. The models used in the analysis presented in this work have been derived using 3- and 4-node beam elements. The cross-sectional displacement field has been described using refined kinematics based on two-dimensional quadratic Lagrange functions, that is, on the L9 elements. More details on these beam models can be found in the work by Carrera and Petrolo [18].

E. Load vector evaluation

The formulation of the external loads can be derived using the Principle of Virtual Displacements, in the same way as in the internal equilibrium equations. If only point loads are considered, the external work can be written as:

$$\delta L_{ext} = \delta\boldsymbol{u}^T|_Q P, \tag{33}$$

where P is the load vector applied to point Q. The weak form of Equation 33 can be achieved by introducing the displacement interpolation:

$$\delta L_{ext} = \delta \boldsymbol{u}_j \Phi_j(x,y,z)|_Q P, \tag{34}$$

Equation 34 can be used to derive the load vector in the case of one-, two- or three-dimensional models:

$$1D \rightarrow \delta L_{ext} = \delta \boldsymbol{u}_{js} \underbrace{F_s(x,z)|_Q N_j(y)|_Q P}_{p^{js}}; \tag{35}$$

$$2D \rightarrow \delta L_{ext} = \delta \boldsymbol{u}_{js} \underbrace{F_s(z)|_Q N_j(x,y)|_Q P}_{p^{js}}; \tag{36}$$

$$3D \rightarrow \delta L_{ext} = \delta \boldsymbol{u}_j \underbrace{N_j(x,y,z)|_Q P}_{p^{js}}; \tag{37}$$

where p^{js} is the fundamental nucleus of the load vector.

F. Global stiffness matrix assembly

The fundamental nucleus can generally be written as $\boldsymbol{k}^{ij\tau s}$, where i and j are related to the FEM approximation while τ and s denote the indexes of the model expansion. When a solid model is considered τ and s disappear. The fundamental nucleus $\boldsymbol{k}^{ij\tau s}$ can be used as a *brick* of the construction of the global stiffness matrix. Figure 3 show how the global stiffness matrix $\boldsymbol{k}$ can be obtained from the fundamental nuclei. The loops on indexes τ and s, once the element and the indexes i and j have been fixed, provide the matrix at the node level. The loops on i and j provide the element matrix, and different elements can be assembled adding the stiffness of the shared nodes. The procedure used for the assembly of the global stiffness matrix can be used to assemble the fundamental nucleus of the load vector, p^{js}. More information on the assembly procedure of structures generally oriented in space can be found in the companion paper written by Carrera and Zappino [20].

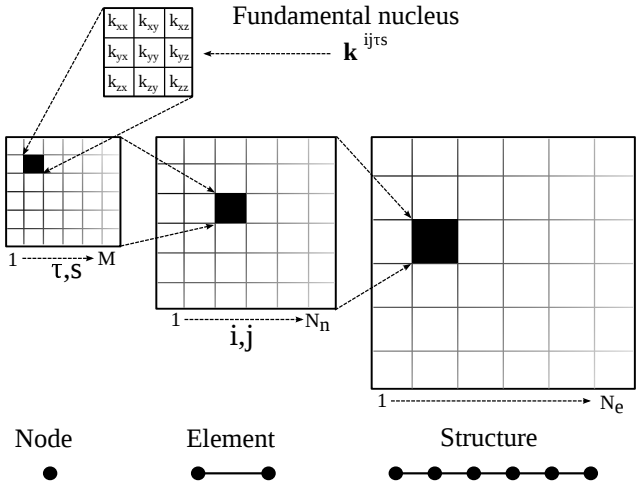

Fig. 3 Global stiffness matrix assembly procedure

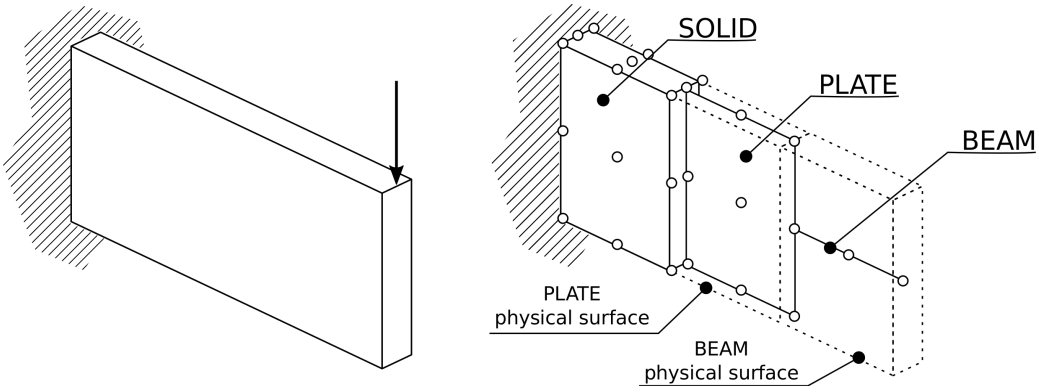

Fig. 4 Example of a model built using elements with different kinematics.

G. Variable kinematic model assembly

The coupling of elements with different kinematics may lead to inconsistency in the displacement and stress fields. Figure 4 shows an example of a simple cantilevered structure and the FEM model for the case in which this structure is investigated using a variable kinematic approach. Solid, plate and beam elements are considered. A classical approach, the use of RBE elements, and the present approach are described in detail in this section.

1. Classical FE model assembly with and without RBE connectors

The use of elements with different kinematics in the same model can produce local effects that may lead to inaccurate results. Figure 5 shows the qualitative results of the problem shown in Figure 4. In this case no special techniques have been used to couple the elements with different kinematics,

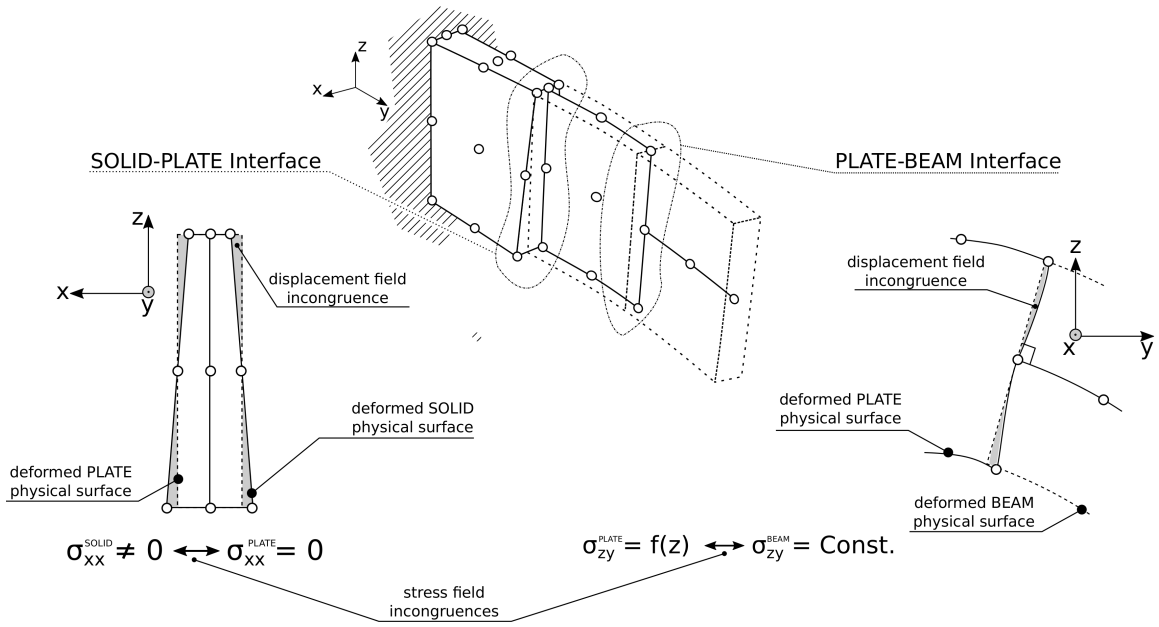

Fig. 5 Classical FE model assembly without RBE connectors.

that is, displacement and rotation equivalence has only been imposed in the connected nodes. The structure is subject to global bending deformation, but local effects may appear at the interface between elements with different kinematic. The displacement field may not be continuous at the interface between solid and plate models, because of the Poisson effect. The upper part of the solid element undergoes traction while the bottom part undergoes compression. This creates restriction and dilatation of the cross-section in the x-direction, respectively. The same behavior cannot be predicted by the plate element, because the kinematic assumptions do not consider any deformation through-the-thickness. As a consequence, σ_{xx} appears at the interface in the solid element, while it does not appear in the plate element.

A similar situation may appear at the interface between the plate and the beam element. In this case, as shown in Figure 5, the beam model forces the cross-section to be undeformed and to follow the rotation predicted at the central node, otherwise, the plate element may predict a deformed cross-section. This may lead to a discontinuous displacement field and to an inconsistency in the shear distribution. In fact, the beam model predicts a constant value, while the plate element may predict a variable shear stress. Rigid Body Elements may be introduced to force the kinematics of the more refined model to follow the kinematics of the lower-order model. Figure 6 shows an example of this situation. When the displacement field is continuous at each interface the stress field

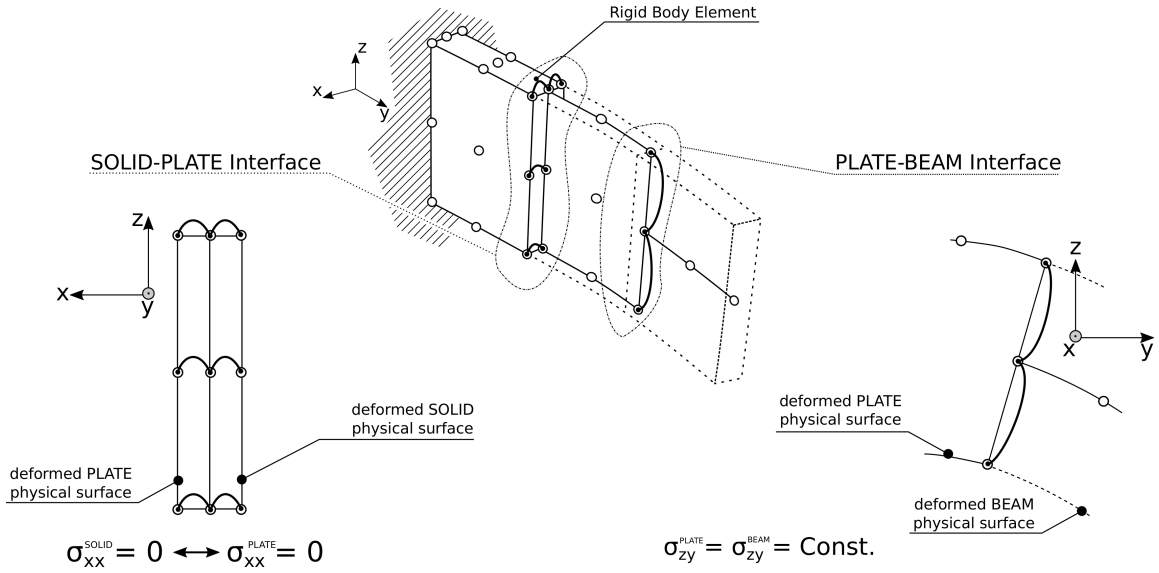

Fig. 6 Classical FE model assembly using Rigid Body Elements.

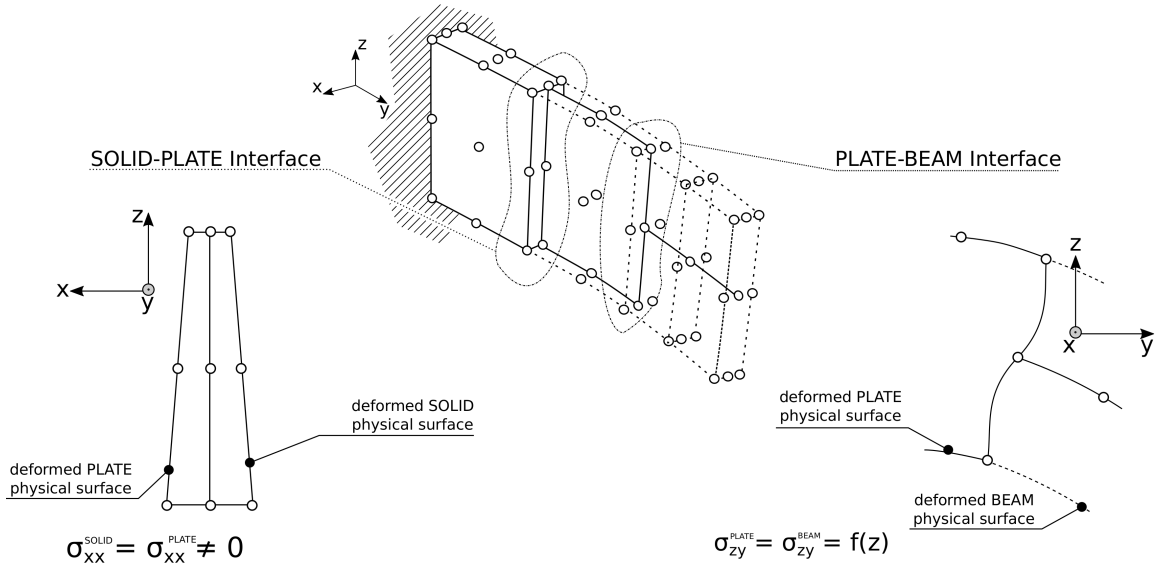

Fig. 7 Present variable kinematic model.

may show oscillations or a local concentration in the transition zone because of the new constraints.

2. Present approach

The refined models introduced in the present paper share a common feature, that is, they all have only displacements as the degrees of freedom. This property allows models with different dimensions to be combined by imposing the equivalence of the displacements at one or more nodes. Figure 7 show the variable kinematic model, of the problem shown in Figure 4, obtained using

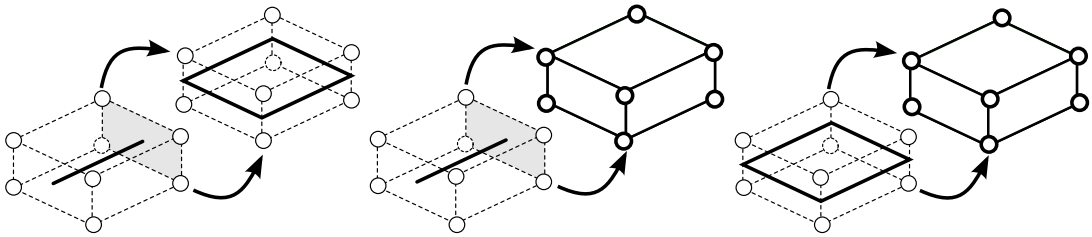

(a) 1D/2D (b) 1D/3D (c) 2D/3D

Fig. 8 Variable kinematic model assembling: the dashed line (- - -) shows the physical domain while the solid line (—) denotes the mathematical domain. Circles (∘) are used to represent the nodes where the unknowns are defined.

the present approach. The capacity of refined plate models to predict the thickness deformation prevents inconsistencies from arising at the solid/plate interface. The displacement and stress fields are also continuous at the plate/beam interface, thanks to the use of higher-order beam models that allow the cross-section to warp in- and out-of-plane. Figure 8 shows the general approach used to assemble the elements, that is, a variable kinematic model assembling. Figure 8a shows how a one-dimensional model can be coupled with a two-dimensional element. Figure 8b shows how a one-dimensional model can be coupled with a three-dimensional element. Finally, a two-dimensional model can be coupled with a solid element as shown in Figure 8c.

III. Numerical results

This section presents some numerical results obtained using the previously introduced variable kinematic model. The first part is devoted to the assessment of the numerical approach. A simple cantilevered beam has been considered, and one-, two- and three-dimensional models have been used to build different numerical models. The second sample concerns the static analysis of a reinforced panel, and, the third case considers the static analysis of a large part of an aircraft structure including a part of the fuselage and the wing structure. The results have been compared with those from literature, when available, while, a reference solution has been created for the other cases using the commercial FEM MSC Nastran® code.

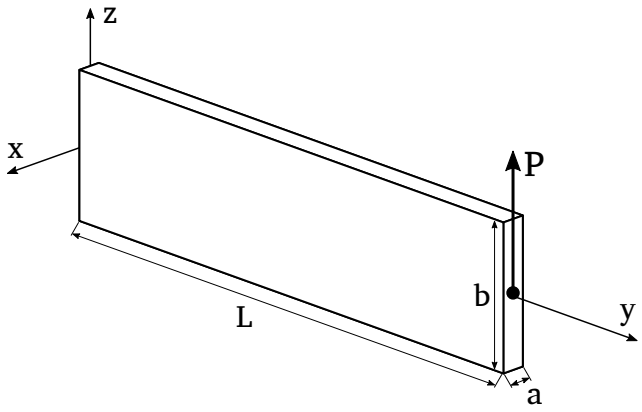

Fig. 9 Reference system and geometry of the cantilevered beam.

A. Assessment of the variable kinematic model

This section considers a cantilevered beam subjected to a bending load. The geometry of the structure, is shown in Figure 9. The beam has a length, L, equal to 8 m. The cross-sectional dimensions are $a = 0.5$ m and $b = 1.5$ m. The structure is clamped at $y = 0$ and a concentrated load, $P = 1000$ N, is applied at the free end at the $a = 0$ and $b = 0$ points. An isotropic material is used, and Young's modulus, E, is considered equal to 70 GPa while the Poisson ratio, ν, is equal to 0.35. The problem has been solved using different numerical models. Three models, with constant kinematics have been considered. The first model, called $1D$, was built using only one-dimensional elements, in this case, 11 B4 elements were used along the beam axis while 6 L9 elements have been used to describe the cross-sectional kinematics. Another model, named $2D$, was built using 126 Q9 (a 21×6 element mesh) quadratic plate elements, and a quadratic approximation was assumed through the thickness. Finally, a fully three-dimensional model, called $3D$, was considered. The solid model was built using 126 (a $21 \times 6 \times 1$ elements mesh) quadratic hexaedronal elements.

Four variable kinematic models have also been considered. The details of these models are reported in Figure 10. Figure 10a shows the model in which one- and two-dimensional elements were used, that is the $1D/2D$ model, in which 66 Q9 plate elements and 6 B4 beam elements were used. The model shown in Figure 10b, model $1D/3D$, was built using 66 H27 solid elements and 6 B4 beam elements. Model $2D/3D$, shown in Figure 10c, was built using 66 H27 solid elements and 66 Q9 plate elements. Finally, a model that uses all three elements is presented as model $1D/2D/3D$, see Figure 10d. In this case the model includes, 36 H27 elements, 36 Q9 elements and

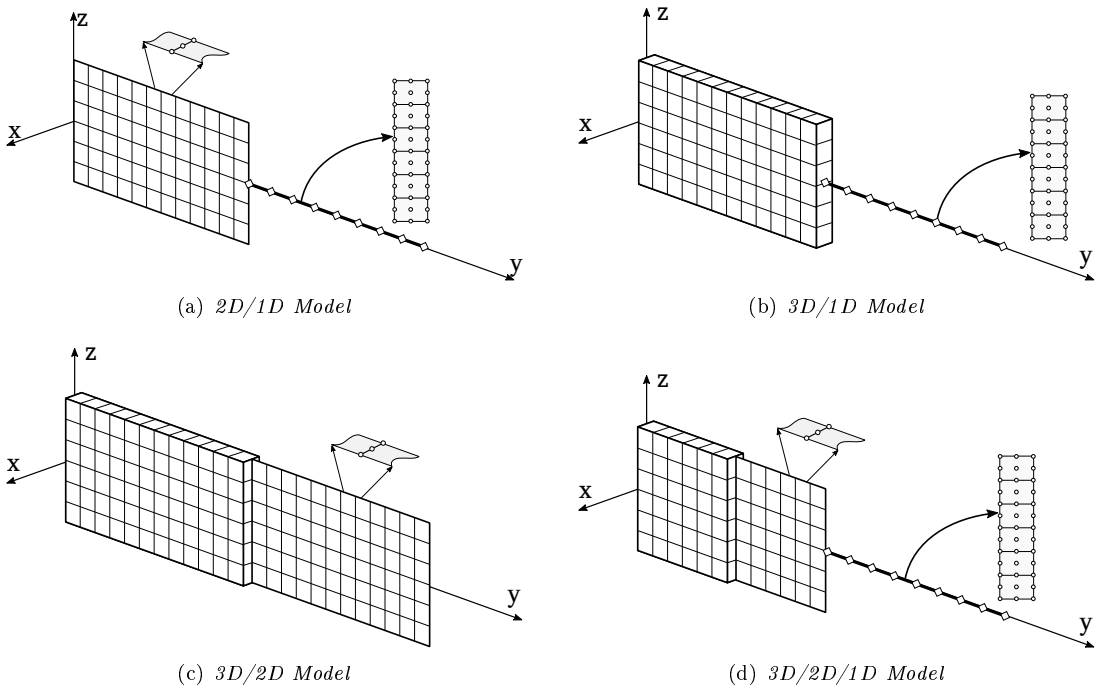

(a) *2D/1D Model* (b) *3D/1D Model*

(c) *3D/2D Model* (d) *3D/2D/1D Model*

Fig. 10 Details of the variable kinematic models.

Model	$u_z \times 10^5$ m	σ_{yy} Pa	τ_{yz} Pa
1D	1.767	37316	2064
2D	1.767	37251	2055
3D	1.767	37251	2055
3D/1D	1.767	37279	2065
3D/2D	1.767	37279	2065
2D/1D	1.767	37279	2065
3D/2D/1D	1.767	37279	2065
Song and Hodges [41]	1.776	37310	2056
Euler-Bernulli	1.734	37333	-
Timoshenko	1.782	37333	1333

Table 1 Vertical displacement, normal stress and shear stress evaluated with different models.

6 B4 elements.

The obtained results have been compared with those obtained using classical models, Euler-Bernulli and Timoshenko beam models and with respect to the results presented by Song and Hodges [41]. Table 1 reports the numerical results obtained using the previously introduced models. The vertical displacement, u_z, was evaluated at the tip in the point at $x = 0$ and $z = 0$. The axial stress,σ_{yy}, was evaluated at $y = 1\ m$, $x = 0$ and $z = -b/2$ while the shear stress,τ_{yz} was evaluated at $y = 1\ m$, $x = 0$ and $z = 0$. The results show that, as expected, all the considered models are

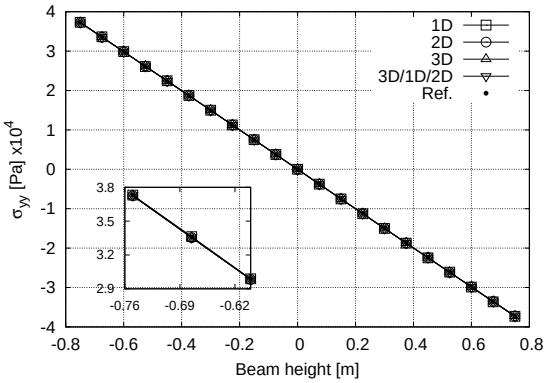

(a) *Axial stress,σ_{yy}, profile*

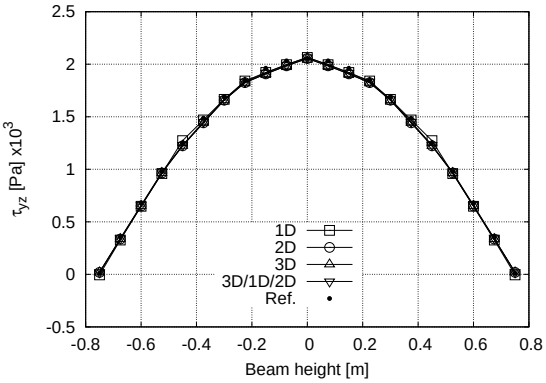

(b) *Shear Stress,τ_{yz}, profile*

Fig. 11 Axial and shear stress profiles evaluated along the beam height at $y = 1$ and $x = 0$.

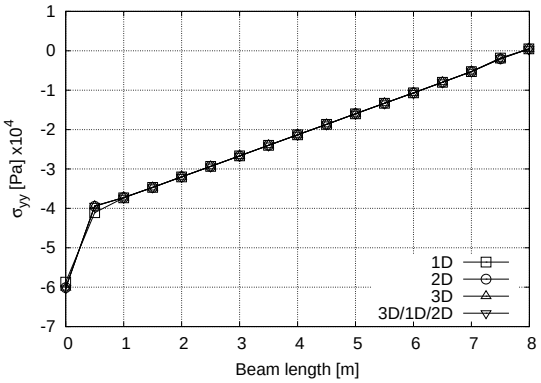

(a) *σ_{yy} axial distribution at $x = 0$ and $z = b/2$*

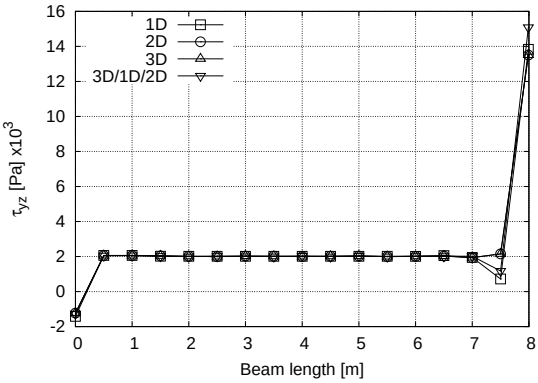

(b) *τ_{yz} axial distribution at $x = 0$ and $z = 0$*

Fig. 12 Axial and shear stress distribution evaluated along the beam axis.

able to provide accurate results. The use of refined beam models allows an accurate value of shear stress to be obtained, and this result cannot be obtained using Euler-Bernulli or Timoshenko beam models. Figure 11 reports the stress profiles evaluated along the z coordinate at $y = 1$ and at $x = 0$. The axial stress, σ_{yy}, is reported in Figure 11a, while the shear stress σ_{yz}, is reported in Figure 11b. All the considered models are able to accurately describe the stress distribution and are able to provide a three-dimensional result. The axial distribution of the normal stress, σ_{yy}, is reported in Figure 12a. All the models are able to describe the linear variation of σ_{yy} and all the models can predict the end-effect due to the constraint. The stress distribution is not affected by the kinematic variation. The same conclusion can be drawn when shear stress is considered, see Figure 12b. Only at the tip of the beam, where the load is applied, it is possible to see a slight difference in the results due to local effects. Again in the case of shear stress, the kinematic variation does not produce any significant effect.

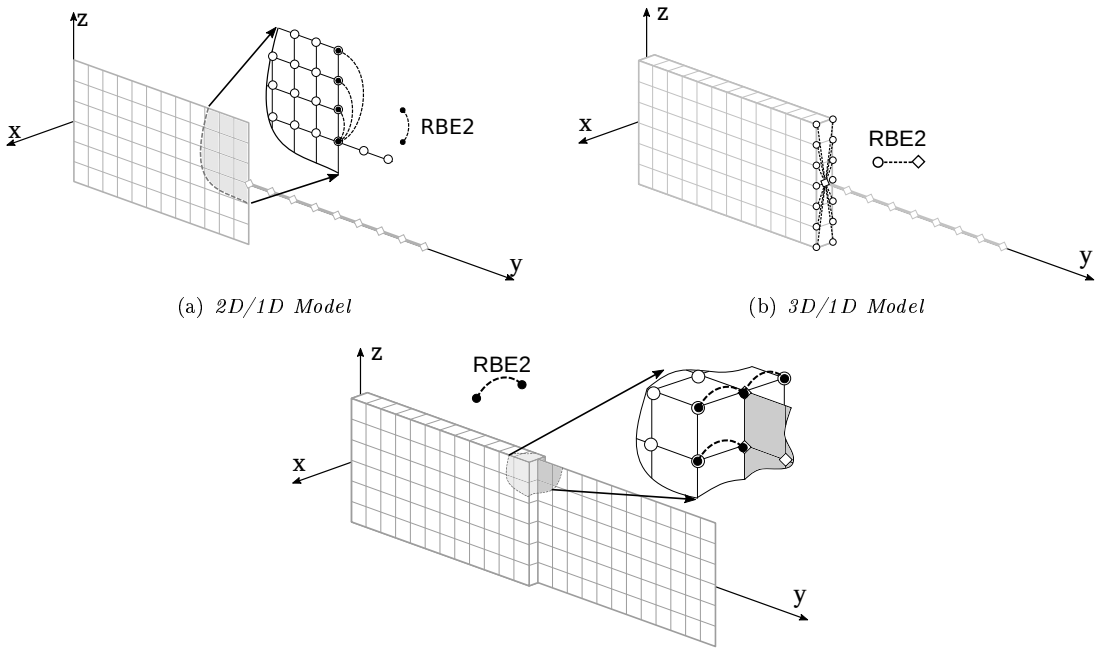

(a) *2D/1D Model* (b) *3D/1D Model*

(c) *3D/2D Model*

Fig. 13 Details of the variable kinematic models obtained using RBE elements.

B. Comparison with classical FEM models

The results obtained in the previous section have been compared with those obtained using the classical tool available in the commercial FEM software MSC Nastran®. Figure 13 shows the three considered models, all of which exploit rigid body elements to connect the elements with different kinematics. Figure 13a shows a model created using beam and plate elements. The model shown in Figure 13b uses solid and beam elements while the model shown in 13c was built using solid and plate elements.

The axial stress, σ_{yy}, and the shear stress, τ_{yz}, evaluated along the beam axis are reported in Figure 14. The results are compared with those obtained using the present 3D/2D/1D model. The qualitative distribution of the axial stress, see Figure 14a, is described properly by all the models although the models built using RBE elements all show local effects at the interface, due to the jump in kinematics, while the present 3D/2D/1D model does not suffer from this phenomenon. When shear stress is considered, see Figure 14b, the advantages of the present 3D/2D/1D models are even more evident. The use of the present approach prevents local effects from arising at the interface and the shear stress is evaluated correctly, even in the portion of the structure where beams are used. The Timoshenko beam model, which is adopted in the commercial software, assumes a

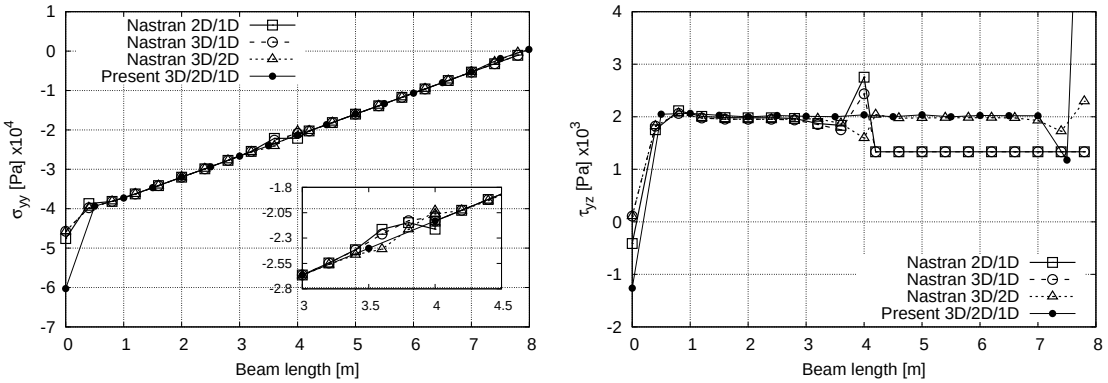

(a) *Axial stress,σ_{yy}, profile* (b) *Shear Stress,τ_{yz}, profile*

Fig. 14 Axial and shear stress profiles evaluated along the beam height at $y = 1$ and $x = 0$.

constant shear distribution over the cross-section that produces an inaccurate result.

Figure 15 shows the shear stress distributions through the thickness of the beam just before and after the models interface. The 2D/1D model is shown in Figure 15a. The results show that the 2D elements overestimate the stress value while the beam elements provide a constant stress value, in agreement with the Timoshenko model, that is, the stress continuity is not respected. However, the results obtained using the present model match perfectly at the interface and are in agreement with the reference solution obtained using a full 3D model. Figure 15b show the shear stress distributions for the 3D/1D model. As in the previous case, the classical models are not able to provide a continuous stress field. The solution obtained with the 3D/2D Nastran model, see 15c, is the most accurate but it still shows a stress discontinuity while the present 3D/2D model provides a continuous stress field.

These findings highlight the limits of the classical approaches when elements with different kinematics have to be connected. The present variable kinematic models may be used to overcome these limitations and to provide accurate results, without the need of additional elements, such as the RBE

C. Reinforced panel analysis

The static analysis of a reinforced panel has been considered in this section. Figure 16 shows the geometry of the panel and the dimensions of the stringers. The square panel has edges of length $L = 1\ m$, while the skin is $0.003\ m$ thick. The panel is rounded off by a rectangular

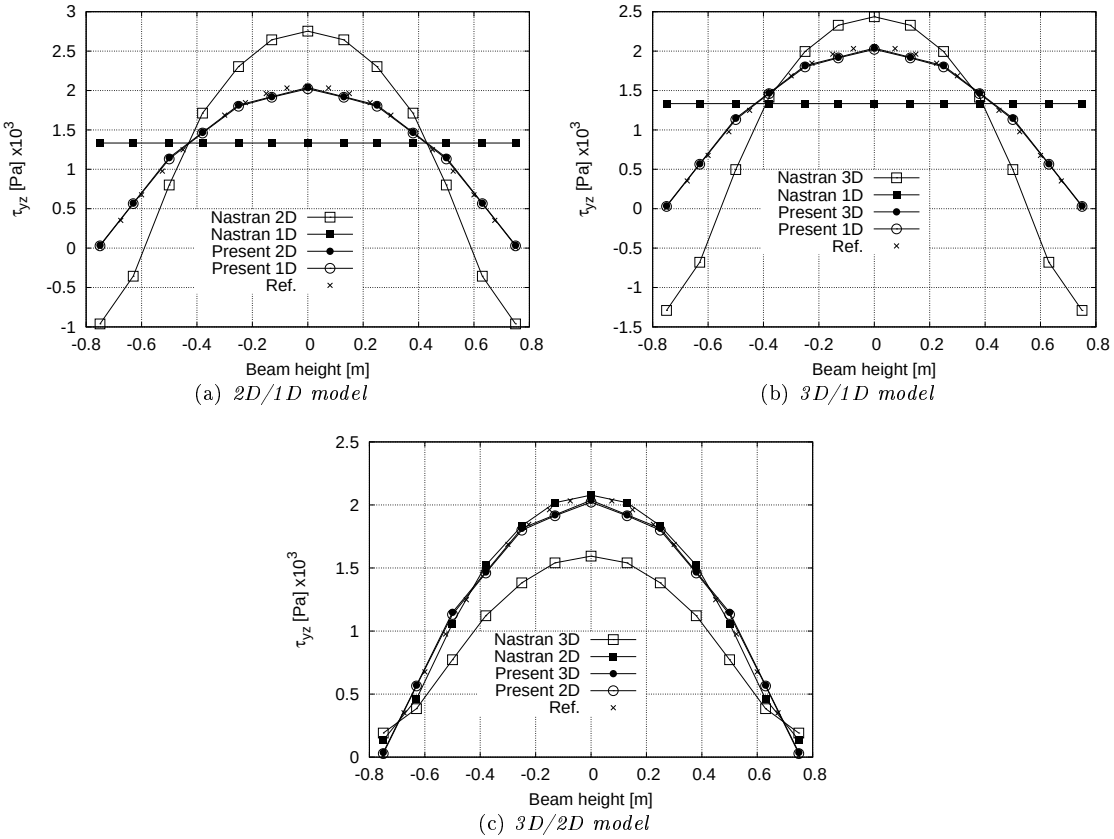

(a) *2D/1D model* (b) *3D/1D model*

(c) *3D/2D model*

Fig. 15 τ_{yz} profiles at the models interface, $x = 0$ and $y = L/2$.

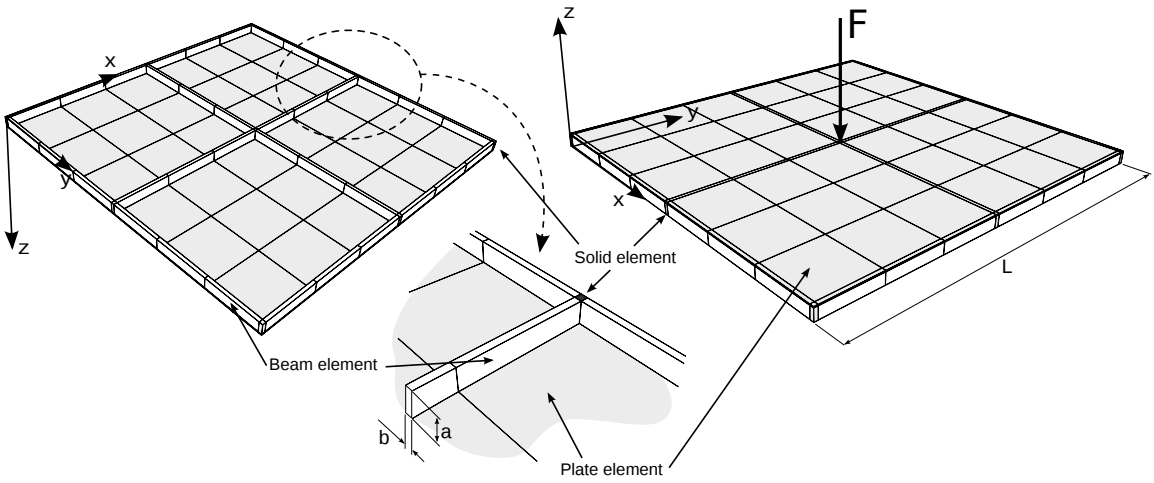

Fig. 16 Reinforced panel geometry

reinforcement and has two stringers in the middle, one in the x direction and the other in the y direction. The dimensions of the cross-section of the reinforcements are $a = 0.03\ m$ and $b = 0.01\ m$. An isotropic material with an elastic modulus of $E = 71.7\ GPa$ and the Poisson ratio $\nu = 0.3$, has been considered. The structure is clamped along the four edges. A point load has been applied

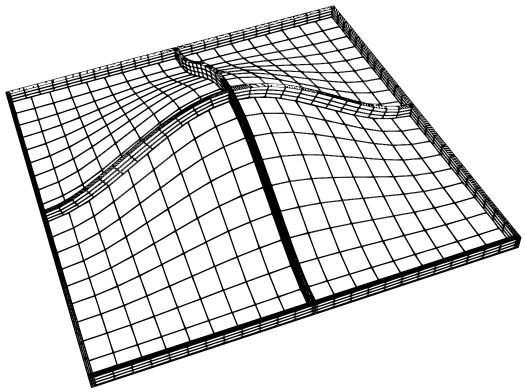

Fig. 17 Reinforced panel deformed configuration.

at the top of the panel in the central point, and the force has a magnitude of $1000N$ in the negative $z-$direction. Figure 16 shows the characteristics of the variable kinematic model. The plate elements are used for the skin, and two non-uniform meshes are considered: the model named MESH1 has a 7×7 elements mesh, while the model named MESH2 uses a mesh of 11×11 elements. A quadratic expansion is used through the thickness of the panel. Quadratic beam elements have been used for the reinforcements, and an L9 element is used over the cross-section. The number of beam elements is related to the skin mesh; the larger the number of elements used over the skin, the larger the number of elements used along the beam axis in order to ensure displacements continuity. A 27-node solid element is used to connect the reinforcements to the skin at the cross-points. The results have been compared with those of a solid model, solved using the commercial FEM MSC Nastran® code. Figure 17 shows the deformed configuration of the panel, from the bottom point of view. Details of the displacements are reported in Figure 18, where the vertical displacement of the panel, evaluated along the central point of the reinforcement in the y-direction, is depicted. The results show that both of the considered models are able to reproduce the results obtained using the full three-dimensional model. The stress field has also been investigated. The axial stress is reported in Figure 19. The results obtained using the variable kinematic models are in agreement with the reference solution. Two stress concentrations can be seen close to the clamped point and in the central part where the stringers are connected. The discontinuity of the stress is due to the post-processing techniques that were adopted. The present paper derives the stresses from the strains using Hook's law in each point, while commercial codes usually average the values obtained

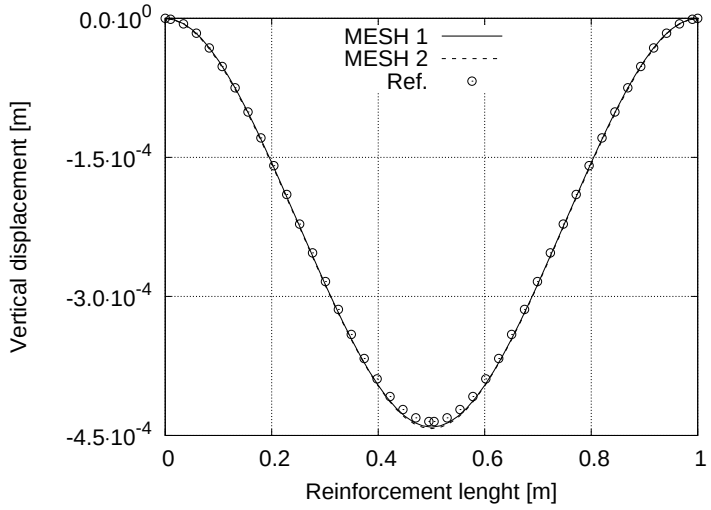

Fig. 18 Vertical displacement of the panel evaluated along the central point of the reinforcement in the y-direction.

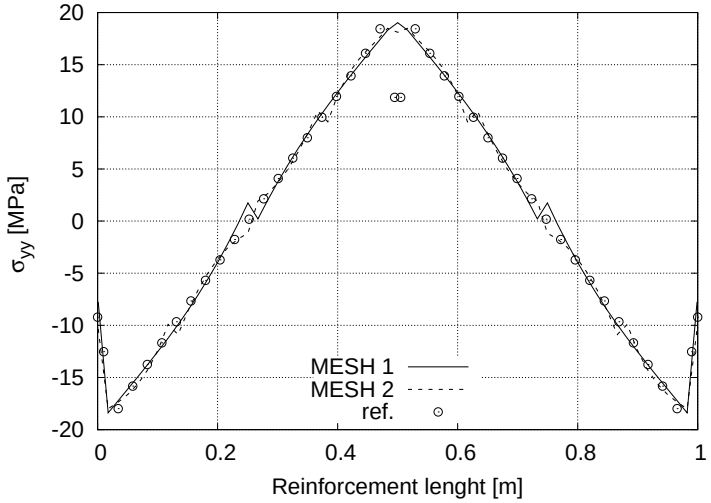

Fig. 19 Axial stress evaluated at the stringer bottom at $x = 0.5$.

in the Gauss points to ensure the continuity. Figure 20 shows the transversal shear stress evaluated along the central point of the reinforcement in the y-direction. The small oscillations in the shear stress value are due to the shear locking correction approach, in this case MITC approach, these can be reduced refining the mesh as shown in the work by Carrera et al. [14]. The results are close to the reference solution but they show some small oscillations. A higher number of beam elements would be required to increase the accuracy. Figure 21 shows the von Mises stress field of the whole structure. The results show the stress concentrations around the reinforcements that are subject to the bending load. The higher solicitations are due to the axial stress, that is, the maximum von

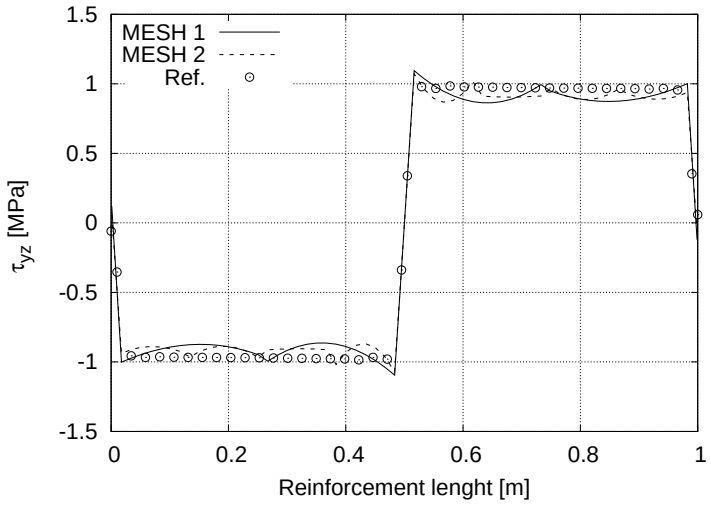

Fig. 20 Shear stress evaluated along the central point of the reinforcement in the y-direction.

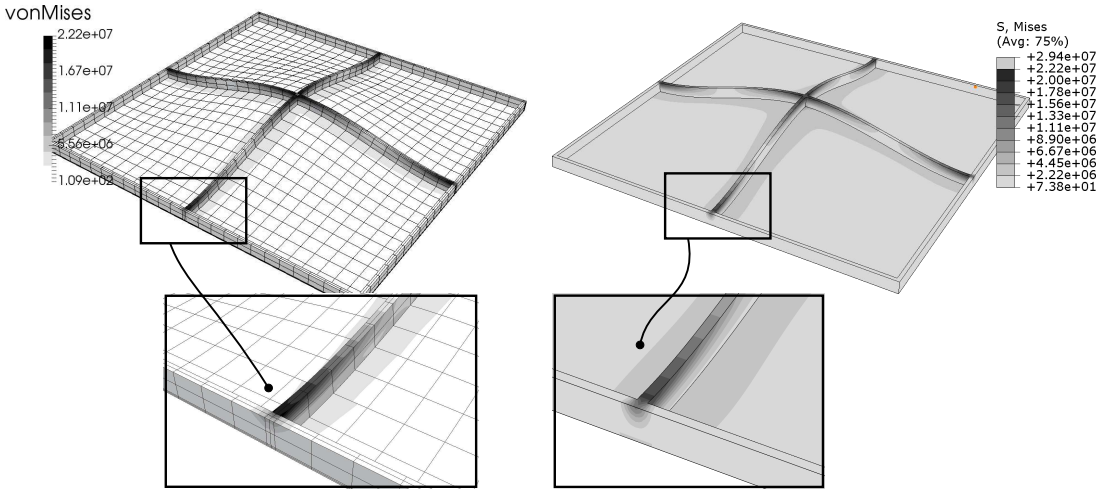

Fig. 21 von Mises stress overview evaluated using the MESH2 model (on the left) and the reference three-dimensional model (on the right).

Mises stress can be found in the bottom part of the stringers that has the maximum values of σ_{yy}.

D. Aircraft structure analysis

This section presents the analysis of a typical aircraft structure, performed using the previously presented variable kinematic model. The structure is shown in Figure 22. It represents a part of a fuselage and includes the wing connection. Ribs, longerons and a thin skin are present in the same structure. The main dimensions of the structure are reported in Table 2. The entire structure is considered to have been built in aluminum alloy, with a Young modulus equal to 71.7 MPa and a Poisson ratio equal to 0.3. The structures is considered clamped the middle plane of the fuselage,

Dimensions $[m]$		
a= 3.000	d= 0.040	g = 0.224
b= 3.160	e= 1.080	h = 0.080
c= 6.000	f= 0.010	i = 0.035

Table 2 Geometrical dimensions of the aircraft component.

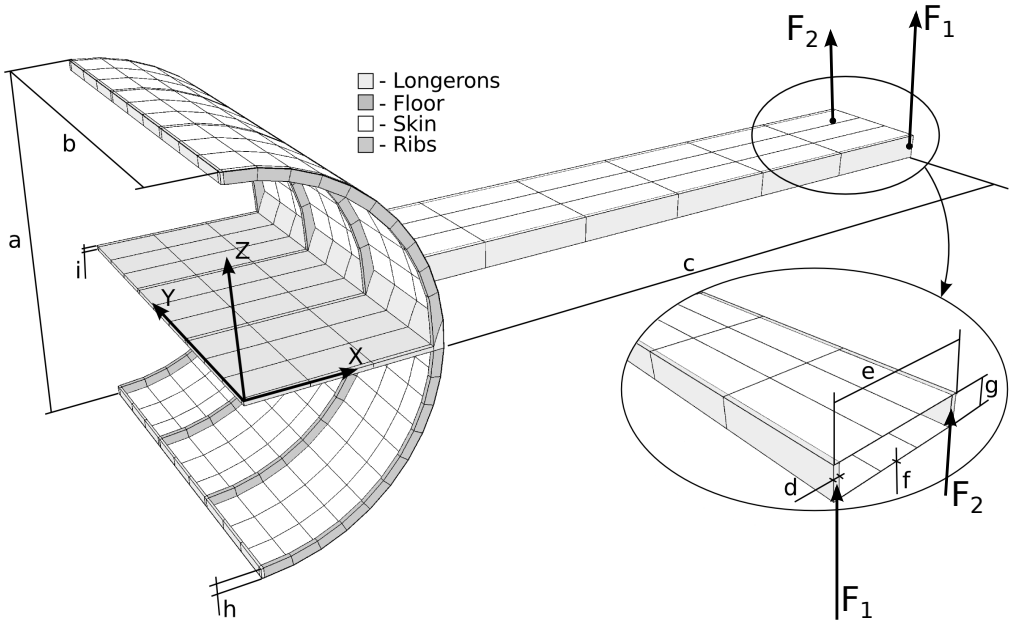

Fig. 22 Aircraft structure considered.

$x = 0\ m$, and at both fuselage extremities, $y = 0\ m$ and $y = 3.160\ m$. Two loads have been placed at the wing tip, as shown in Figure 22; F_1 is equal to 5000 N while F_2 has a magnitude of 2000 N. The whole fuselage structure has been modeled using one- and two-dimensional elements. The fuselage is considered as a beam with a variable cross-section in order to consider the effects of the ribs. Figure 23 shows some details of the cross-sectional mesh used in the models, 23 L9 elements have been used in the circumferential direction while 1 L9 element has been used through the thickness of the skin and of the ribs. 3 L9 elements have been used for the fuselage deck. The wing longerons are also considered as beams. The upper and lower skins of the wing are considered as plate elements. Two models, derived using the present approach, have been considered: the first, referred to as the *present model* and presented in Figure 24a, has a coarse mesh, while the *present refined model*, see Figure 24b, has a more refined mesh and therefore a larger number of DOFs. The results have been compared with a solid model derived using the commercial MSC Nastran ® code.

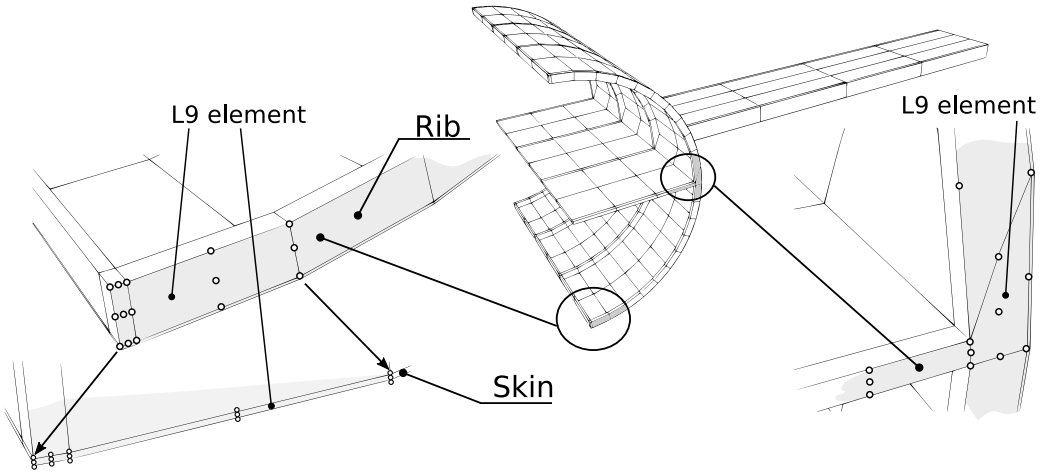

Fig. 23 Details of the cross-sectional mesh, both the skin and the ribs have been modeled using L9 elements.

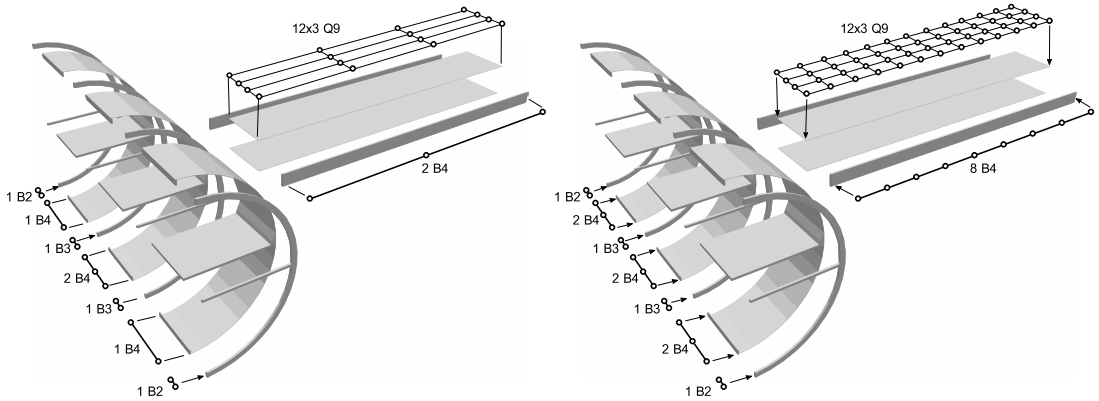

(a) *Present model* (b) *Present refined model*

Fig. 24 Details of the two models of the aircraft structure.

The displacement field evaluated using the present refined model is presented in Figure 25. The loads create both bending and torsional deformation of the wing. Details of the displacement field are shown in Figures 26 and 27. Figure 26 shows the vertical displacement, evaluated at the central point of the frontal wing longeron. The results of both of the present models appear to be accurate, compared with those of the reference model. The same behavior can be observed in Figure 27, where the radial displacement, evaluated at the outer radius of the second rib, is shown. Again in this case, the results of both the coarse and the refined present models are in agreement with those from the reference solution. The analysis of the displacement field shows that a coarse mesh is enough to reach an accurate solution. The stress field has also been analyzed. Figure 28 shows the axial stress evaluated at the top of the frontal wing longeron. The results show that the present model is able

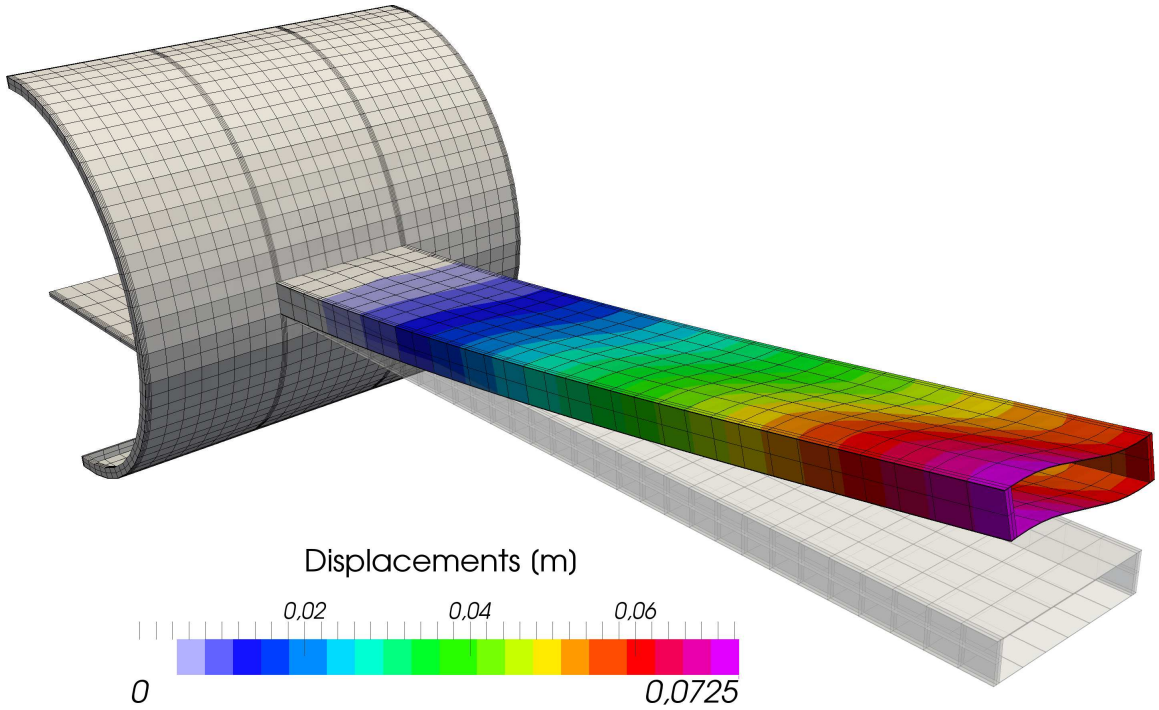

Fig. 25 Three-dimensional displacement field.

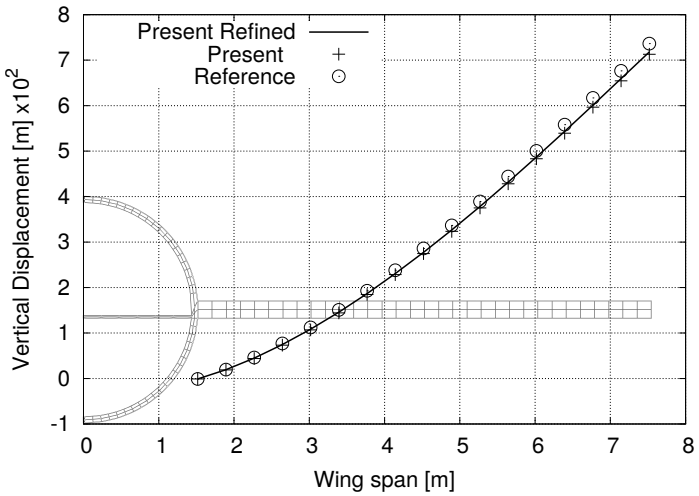

Fig. 26 Vertical displacement evaluated at the center of the frontal wing longeron.

to describe the solution accurately, but only when a refined mesh is used. The coarse mesh, which considers only two beam elements along the longheron, catches the general distribution, but can introduce a large error locally. Figure 29 shows the transversal shear stress evaluated at the center of the frontal wing longeron. The results obtained using the refined mesh are globally accurate, but they show some small oscillations. Finally, the circumferential stress evaluated at the outer radius of the second rib is presented in Figure 30. The results obtained using the present models are able

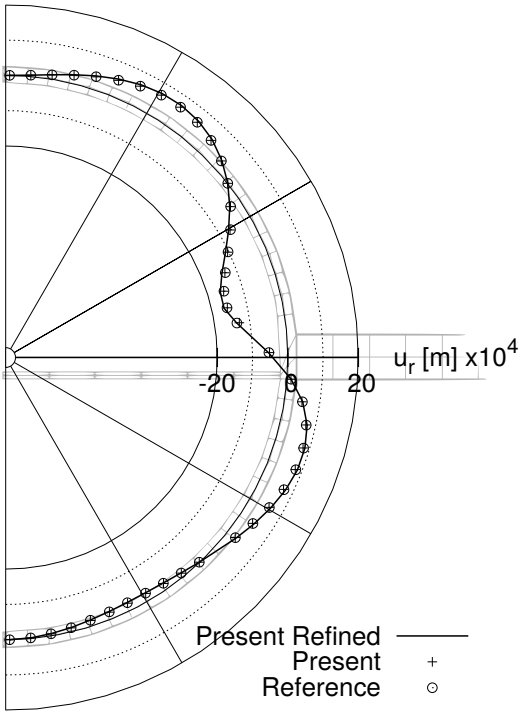

Fig. 27 Radial displacement evaluated at the outer radius of the second rib.

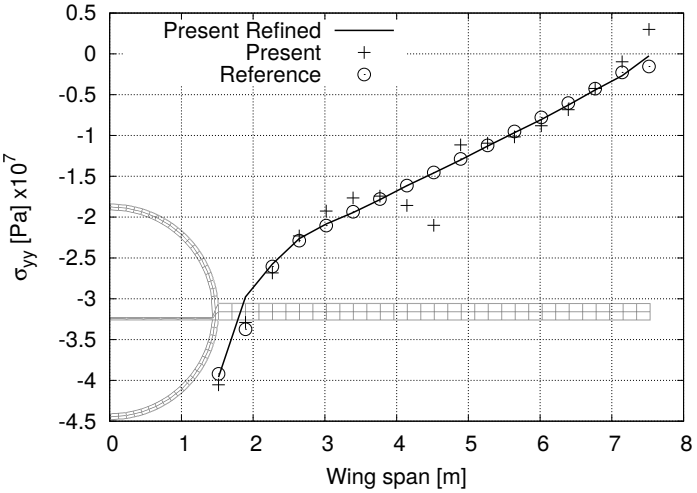

Fig. 28 Assial stress evaluated at the top of the frontal wing longeron.

to accurately describe the stress distribution. A perfect matching can be seen along almost all of the half circumference. Some small discrepancies appear close to the fuselage/wing connection where, a complex three-dimensional stress field, is present. The use of three dimensional elements in this part could lead to a perfect matching. From the results, it is possible to see that the model that uses a coarse mesh is able to provide accurate results in terms of displacements but not in terms of stress field. An accurate description of the stress field can only be achieved using a more refined mesh. In

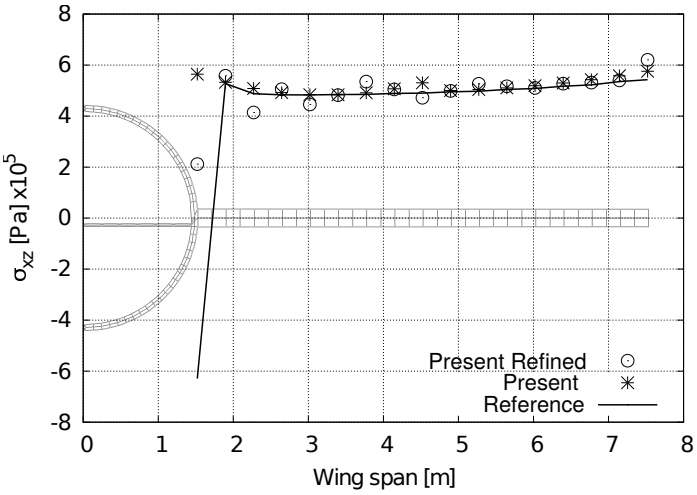

Fig. 29 Transversal shear stress evaluated at the centre of the frontal wing longeron.

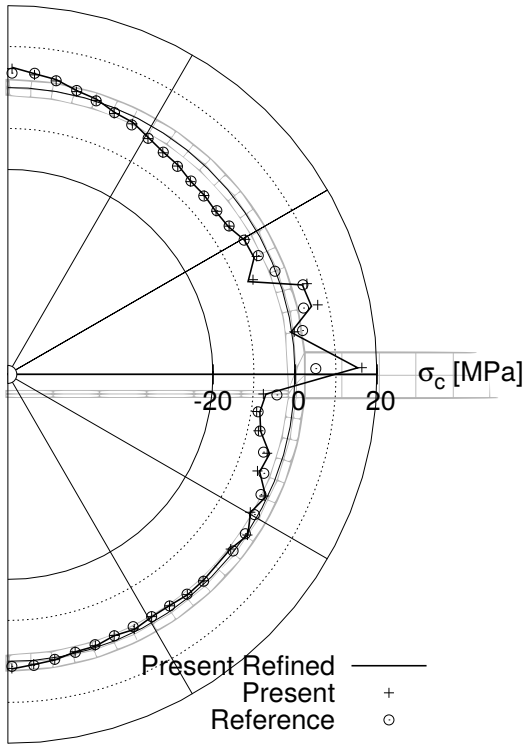

Fig. 30 Circumferential stress distribution evaluated at the outer radius of the second rib.

this case, the stresses are predicted accurately in both the wing and the fuselage structures.

IV. Conclusions

The present work presents the use of a refined variable kinematic model for the analysis of complex structures such as reinforced thin-walled structures. The Unified Carrera Formulation has been used to derive refined one-, two- and three-dimensional models in compact form. The use of

a displacement-based kinematic approximation has allowed models with different kinematics to be connected in order to obtain a variable kinematic model. Different structures have been considered in order to highlight the capabilities of the present approach. The findings show that the present model overcomes the limitations introduced by classical FEM models. It provides a much more accurate description of the interface between elements with different kinematics. Such accuracy cannot be reached using classical FEM models, even if RBE elements are adopted.

The results of the analysis of a simple beam structure have shown the accuracy of the present model. The results are not affected by the transition between different kinematics, and continuity of the displacement and stress fields is guaranteed. The same accuracy has not been reached using classical models, which showed local stress oscillations due to the kinematic variation.

The model was then used to analyses a reinforced panel. In this case, the variable kinematic model was used to represent a complex structure. The capabilities of the present approach allowed the geometry of the panel to be represented accurately, and in this way the accuracy of the three-dimensional models was preserved where required, e.g. at the stringer intersection, while the beam model properties were exploited in the reinforcements.

Finally, a complex aircraft structure has been considered. The obtained results show how the present approach can be used to investigate complex structures. Accuracy of the results has been shown, that is, the use of refined one- and two-dimensional models provides a three-dimensional stress field.

In short, the present approach allows refined structural models with different kinematics to be joined together. The models obtained using this approach preserve the accuracy of the refined structural models, but also make it possible to study complex structures, which usually requires classical FEM models.

References

[1] Argiris, 1965. Matrix analysis of three-dimensional elastic media small and large displacements. AIAA Journal 3 (1), 45–51.

[2] Argiris, J. M., Kelsey, S., 1960. Energy theorems and structural analysis. Butterworths.

[3] Ben Dhia, H., 1998. Multiscale mechanical problems: the arlequin method. Comptes Rendus de l'Academie des Sciences Series IIB Mechanics Physics Astronomy 326 (12), 899–904.

[4] Ben Dhia, H., Rateau, H., 2005. The arlequin method as a flexible engineering tool. International journal for numerical methods in engineering 62 (11), 1442–1462.

[5] Biscani, F., Giunta, G., Belouettar, S., Carrera, E., Hu, H., 2011. Variable kinematic beam elements coupled via Arlequin method. Composite Structures 93, 697–708.

[6] Blanco, P. J., Feijóo, R. A., Urquiza, S. A., 2008. A variational approach for coupling kinematically incompatible structural models. Computer Methods in Applied Mechanics and Engineering 197 (17-18), 1577–1602.

[7] Bruhn, E. F., 1973. Analysis and design of flight vehicle structures. Tri-State Offset Company.

[8] Carrera, E., 1995. A class of two dimensional theories for multilayered plates analysis. Atti Accademia delle Scienze di Torino, Memorie Scienze Fisiche 19-20, 49–87.

[9] Carrera, E., 1999. Multilayered Shell Theories that Account for a Layer-Wise Mixed Description. Part I. Governing Equations. AIAA Journal 37, 1107–1116.

[10] Carrera, E., 1999. Multilayered Shell Theories that Account for a Layer-Wise Mixed Description. Part II. Numerical Evaluations. AIAA Journal 37, 1117–1124.

[11] Carrera, E., Brischetto, S., Nali, P., 2011. Plates and Shells for Smart Structures: Classical and Advanced Theories for Modeling and Analysis. John Wiley & Sons.

[12] Carrera, E., Cinefra, C., Nali, P., 2010. Mitc technique extended to variable kinematic multilayered plate elements. Composite Structures (92), 1888–1895.

[13] Carrera, E., Cinefra, M., , Petrolo, M., Zappino, E., 2014. Finite Element Analysis of Structures Through Unified Formulation. John Wiley & Sons.

[14] Carrera, E., de Miguel, A., Pagani, A., 2017. Extension of MITC to higher-order beam models and shear locking analysis for compact, thin-walled and composite structures International Journal for Numerical Methods in Engineering, In Press, 1–14.

[15] Carrera, E., Giunta, G., Petrolo, M., 2011. Beam Structures: Classical and Advanced Theories. John Wiley & Sons Ltd.

[16] Carrera, E., Pagani, A., Petrolo, M., 2013. Use of Lagrange multipliers to combine 1D variable kinematic

finite elements. Computers & Structures 129, 194–206.

[17] Carrera, E., Pagani, A., Petrolo, M., Zappino, E., 2015. Recent developments on refined theories for beams with applications. Mechanical Engineering Reviews, Bulletin of the Japan Society of Mechanical Engineers JSME 2 (2), 14–00298–14–00298.

[18] Carrera, E., Petrolo, M., 2012. Refined Beam Elements With Only Displacement Variables and Plate/Shell Capabilities. Meccanica 47 (3), 537–556.

[19] Carrera, E., Zappino, E., 2013. Full Aircraft Dynamic Response by Simplified Structural Models. In: Proceedings 54rd AIAA/ASME/ASCE/AHS/ASC Structures, Structural Dynamics, and Materials Conference (SDM).

[20] Carrera, E., Zappino, E., 2015. Carrera Unified Formulation for Free-Vibration Analysis of Aircraft Structures. AIAA Journal 54 (1), 280–292.

[21] Cofer, W., Will, K., 1991. A three-dimensional, shell-solid transition element for general nonlinear analysis. Computers and Structures 38 (4).

[22] da Silva, V. D., 1995. Mechanics and strenght of materials. Springer.

[23] Dávila, C. G., apr 1994. Solid-to-shell transition elements for the computation of interlaminar stresses. Computing Systems in Engineering 5 (2), 193–202.

[24] Edalat, P., Khedmati, M. R., Guedes Soares, C., 2013. Free Vibration and Dynamic Response Analysis of Stiffened Parabolic Shells using Equivalent Orthotropic Shell Parameters. Latin American Journal of Solids and Structures 10, 747–766.

[25] Edward, A. S., Samer, A. T., 2000. A fnite element model for the analysis of stiffened laminated plates. Computers and Structures 20, 369–383.

[26] Euler, L., 1744. De curvis elasticis. Lausanne and Geneva: Bousquet.

[27] Garusi, E., Tralli, A., 2002. A hybrid stress-assumed transition element for solid-to-beam and plate-to-beam connections. Computers and Structures 80 (2), 105–115.

[28] Gmür, T. C., Kauten, R. H., may 1993. Three-dimensional solid-to-beam transition elements for structural dynamics analysis. International Journal for Numerical Methods in Engineering 36 (9), 1429–1444.

[29] Gmür, T. C., Schorderet, A. M., 1993. A set of three-dimensional solid to shell transition elements for structural dynamics. Computers and Structures 46 (4).

[30] Hoseini, H. S., Hodges, D. H., jan 2016. Joining 3-D Finite Elements to Variational Asymptotic Beam Models. In: 57th AIAA/ASCE/AHS/ASC Structures, Structural Dynamics, and Materials Conference. AIAA SciTech Forum. American Institute of Aeronautics and Astronautics.

[31] Liao, C. L., Reddy, J. N., Engelstad, S. P., aug 1988. A solid-shell transition element for geometrically

non-linear analysis of laminated composite structures. International Journal for Numerical Methods in Engineering 26 (8), 1843–1854.

[32] Love, A. E. H., 1888. The Small Free Vibration and Deflection of a Thin Elastic Shell. Philosophical Transactions of the Royal Society of London A 179, 491–546.

[33] Luan, Y., Ohlrich, M., Jacobsen, F., 2011. Improvements of the smearing technique for cross-stiffened thin rectangular plates. Journal of Sound and Vibration 330, 4274–4286.

[34] McCune, R. W., Armstrong, C. G., Robinson, D. J., 2000. Mixed-dimensional coupling in Finite element models. International Journal for Numerical Methods in Engineering 49 (6), 725–750.

[35] Mindlin, R. D., 1951. Influence of rotatory inertia and shear on flexural motions of isotropic elastic plates. ASME Journal of Applied Mechanics 18, 31–38.

[36] Monaghan, D. J., Doherty, I. W., Mc Court, D., Armstrong, C. G., 1998. Coupling 1D Beams to 3D Bodies. In: 7th International Meshing Roundtable, Sandia National Laboratories. pp. 285–293.

[37] Mustafa, B. A., Ali, R., 1987. Prediction of natural frequency of vibration of stiffened cylindrical shells and orthogonally stiffened curved panels. Journal of Sound and Vibration 113, 317–327.

[38] Reissner, E., 1945. The effect of transverse shear deformation on the bending of elastic plates. ASME Journal of Applied Mechanics 12, 68–77.

[39] Robinson, T. T., Armstrong, C. G., Fairey, R., 2011. Automated mixed dimensional modelling from 2D and 3D CAD models. Finite Elements in Analysis and Design 47 (2), 151–165.

[40] Shim, K. W., Monaghan, D. J., Armstrong, C. G., 2002. Mixed dimensional coupling in finite element stress analysis. Engineering with Computers 18 (3), 241–252.

[41] Song, H., Hodges, D. H., 2010. Rigorous joining of advanced reduced-dimensional beam models to {2D} finite element models. In: 51st AIAA/ASME/ASCE/AHS/ASC Structures, Structural Dynamics and Materials Conference. No. April. 12 - 15 April 2010, Orlando, Florida, pp. 1–18.

[42] Surana, K. S., 1980. Transition finite elements for threeâĂŘdimensional stress analysis. International Journal for Numerical Methods in Engineering 15 (7).

[43] Surana, K. S., 1982. Geometrically non-linear formulation for the three dimensional solid-shell transition finite elements. Computers and Structures 15 (5).

[44] Timoshenko, S. P., 1921. On the corrections for shear of the differential equation for transverse vibrations of prismatic bars. Philosophical Magazine 41, 744–746.

[45] Turner, M. J., Clough, R. W., Martin, H. C., Topp, L. J., 1956. Stiffness and Deflection Analysis of Complex Structures. Journal of the Aeronautical Sciences 23 (9), 805–823.

[46] Washizu, K., 1968. Variational methods in elasticity and plasticity. Oxford: Pergamon Press.

[47] Yu, W., Hodges, D. H., Jimmy, C., 2012. Variational Asymptotic Beam Sectional Analysis – An Updated Version. International Journal of Engineering Science 59, 40–64.

[48] Yu, W., Volovoi, V. V., Hodges, D. H., Hong, X., 2002. Validation of the variational asymptotic beam sectional analysis. AIAA Journal 40, 2105–2113.

[49] Zienkiewicz, O. C., Taylor, R. L., 2000. The Finite Element Method for Solid and Structural Mechanics, sixth edit Edition. Elsevier Butterworth-Heinemann, Oxford.